

Coupled-channels study of antiproton-proton reactions

G. Q. Liu* and Frank Tabakin

Department of Physics and Astronomy, University of Pittsburgh, Pittsburgh, Pennsylvania 15260

(Received 14 July 1989)

Low energy antiproton-proton elastic, charge exchange, charged pion, and charged kaon production reactions are studied in a coupled-channels model. The need for a coupled-channels approach to antiproton-proton reactions is first demonstrated. Meson exchange potentials describe the long-range $\bar{N}N$ interaction; smooth phenomenological forms are used for the $\bar{N}N$ interaction at short distances. Effective channels are introduced to simulate strong absorptive effects, such as multimeson production processes. Transition potentials for kaon and pion production are derived in coordinate space and shown to include an important spin-times-derivative coupling form. These transition potentials, along with a one-boson-exchange model with effective absorptive channels, are used to determine the role of multistep processes of the type $\bar{\pi}\pi \leftrightarrow \bar{p}p \leftrightarrow \bar{n}n \leftrightarrow \bar{K}K$. Control over such coupled-channels effects is sought as a step toward unfolding short-distance quark effects in a reliable way. The $\bar{p}p$ elastic and charge exchange differential cross sections at three $\bar{p}p$ laboratory momenta (780, 690, and 590 MeV/c) are examined first, since $\pi^- \pi^+$ and $K^- K^+$ data also exist at these energies. Results are then presented that manifest strong coupling effects, especially between the pion and kaon production channels. Based on that result, a full coupled-channels fit to the $\bar{p}p$, $\bar{n}n$, $K^- K^+$, and $\pi^- \pi^+$ data is presented and analyzed.

I. INTRODUCTION

A major feature of antiproton reactions is the large annihilation of the $\bar{p}p$ system to multihadron final states. Elastic, charge exchange, and exclusive two-hadron production processes also occur, amidst the dominant annihilation. Thus, in contrast to the nucleon-nucleon (NN) case, antinucleon-nucleon ($\bar{N}N$) reactions always involve strong absorption, which makes this case simpler from the absorptive disk view, but more complicated in that many competing processes occur simultaneously. Now that precision data for a range of low energy $\bar{p}p$ exclusive reactions are under intensive experimental study at LEAR, it is timely to examine this problem.

Other authors¹⁻¹⁰ have already explored the $\bar{p}p$ elastic and charge exchange processes using an optical plus one-boson-exchange potential (OBEP) approach and have produced good fits to $\bar{p}p$ elastic, charge exchange, and annihilation data. In some cases,^{11,12} coupled-channels calculations have been initiated. However, Kageyama *et al.*¹³ assert that their measured $\bar{p}p$ elastic and charge exchange differential cross sections are not in satisfactory agreement with either the Paris, Nijmegen, or Dover and Richard models and they suggest a reanalysis of the present $\bar{N}N$ models. In previous coupled-channels approaches, meson production channels have not yet been fully explored.

In our paper, we analyze the Kageyama *et al.*¹³ (and also the recent Kunne *et al.*^{14,15}) measurements of $\bar{p}p$ elastic and charge exchange with a coupled-channels (CC) approach, that now includes the $\pi^- \pi^+$ and $K^- K^+$ channels. The nature of the interactions and coupling potentials are discussed from a baryon exchange viewpoint and annihilation is included by means of effective channels, following the Nijmegen philosophy.^{5,4}

Our coupled-channels fit to the above set of elastic, charge exchange, and meson production data is then presented and the total and differential cross sections, the partial cross sections, and the partial wave amplitudes are examined in detail.

The first step we take is to fit only the $\bar{p}p$ elastic and charge exchange differential cross sections of Kageyama *et al.*,¹³ with a truncated CC model involving a channel space of only elastic, charge exchange, and effective annihilation channels. Then the $\pi^- \pi^+$ and $K^- K^+$ channels are added in sequentially and fit to existing meson production data. (Since accurate polarization and spin correlations data were not available until recently,¹⁴ we do not at this stage include spin observables in our fitting, but fix our parameters by the best match to known differential and total cross-sections.) The role of adding in the meson production channels proves to be quite significant, especially the mutual effect between the kaon and pion channels. Since multistep processes of the type $\bar{\pi}\pi \leftrightarrow \bar{p}p \leftrightarrow \bar{n}n \leftrightarrow \bar{K}K$ prove to be so significant, a larger CC space was used to refit all the data, i.e., the meson production data were used directly in a CC calculation including elastic, charge exchange, charged pion, and charged kaon pair production and effective annihilation channels. (Note that we have not included a $\bar{\pi}\pi \leftrightarrow \bar{K}K$ transition via K^* exchange. It has also been pointed out to us that the $\bar{K}K$ diagonal interaction might be significantly stronger than for the $\pi\pi$ case, because of ω exchange. These issues are under study.) This paper is of exploratory nature and our calculations are presented for only three \bar{p} momenta 780, 690, and 590 MeV/c where simultaneous measurements on $\bar{p}p$ elastic, charge exchange, and charged meson production differential cross sections are available. Similar CC calculations for $\bar{\Lambda}\Lambda$ production and for $\bar{p}p$ reactions at low energies are also underway.^{16,17}

II. THE COUPLED-CHANNELS APPROACH

A. The data indicates the need for coupled channels

Even before formulating a coupled-channels (CC) approach, it is clear from existing data¹³ that multistep effects need to be treated. For example, look at Fig. 1, where the differential cross sections for the $\bar{p}p \rightarrow \bar{p}p$ (elastic), for $\bar{p}p \rightarrow \bar{n}n$ (charge exchange), and for charged meson production ($\bar{p}p \rightarrow \pi^- \pi^+$, $\bar{p}p \rightarrow K^- K^+$) are given at 780 MeV/c. The elastic and charge exchange data is given in millibarns, and the charged pion and kaon production data are in microbarns. The main point is that these cross sections are often comparable within a factor of 10, especially at back angles. If cross sections are even

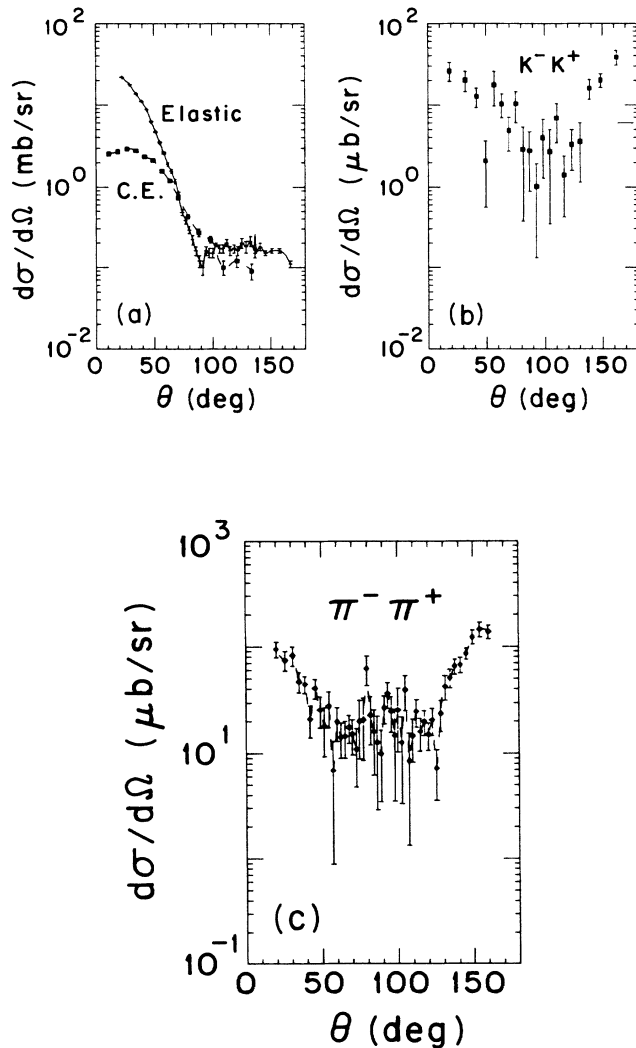


FIG. 1. Differential $\bar{p}p$ cross sections at $p_{\text{lab}} = 780$ MeV/c (lab kinetic energy: 281 MeV). (a) Elastic and charge exchange data. The data are that of Eisenhandler *et al.* (Ref. 32). Kageyama *et al.* (Ref. 13), plus some from Jayet *et al.* (Ref. 33). (b) the $K^- K^+$ data of Eisenhandler *et al.* (Ref. 32); and (c) the Eisenhandler *et al.* (Ref. 32) $\pi^- \pi^+$ data.

within factors of 50, the corresponding *amplitudes* are similar enough to interfere. Therefore, multistep processes such as $\bar{p}p \rightarrow \bar{K}K \leftrightarrow \bar{n}n \leftrightarrow \pi^- \pi^+$ are likely to occur. (One can view these competitive channels as a set of coupled pendula.)

The general reasons for adopting a coupled-channels approach are therefore (1) the data for various channels are comparable and hence multistep processes are likely; (2) the unfolding of quark effects and resonances from hadron exchange requires that we have control over initial- and final-state effects; (3) the unfolding of possibly universal polarization effects, which are related to a common $\bar{s}s$ production mechanism,¹⁸ requires full understanding of the dynamics, especially initial- and final-state effects. Note the back angle buildup of the charged meson production cross sections and the “bump-dip” angular structure of the charge exchange.

B. Basis states and potentials

To simulate annihilation, we adopt the Nijmegen⁴ approach of introducing effective channels, instead of optical potentials, to absorb flux. The effective channel approach offers a physically realistic simulation of the flux lost to various multihadron final states. (The production of ρ, ω two-body final states, for example, might contribute significantly to the dominant $\bar{p}p$ five-pion production channel.) Correspondingly, the Nijmegen interactions yield reasonable analytic and unitarity properties, with meaningful ranges.

We therefore couple four effective two-particle channels, of mass M_i , $i=1,4$, to the antibaryon-baryon ($\bar{B}B$) system (two for $I=0$, two for $I=1$). Of the two for each I , one channel has a lower, the other a higher mass, so each affects the associated $\sqrt{s} = 2M_i$ regions; we call these effective baryon (EB) channels EB_1, EB_2, EB_3 , and EB_4 . In addition, four similar effective meson (EM) channels, EM_i , are available in our code to absorb flux directly from antimeson-meson ($\bar{M}M$) states; as a first study these were kept off. A schematic description of the CC model is displayed in Fig. 2.

As more knowledge about inelastic processes accumulates, more channels can be included in the basis $|\alpha\rangle$, and the effective channel spaces $|\text{EB}_i\rangle$ and $|\text{EM}_i\rangle$ will play a smaller role. However, at this stage, it is essential to include such a coupled-channels mechanism to absorb flux. Although still highly phenomenological, the coupled-channels approach does at least have the correct physical structure for describing the highly absorptive $\bar{p}p$ reactions. It is hoped that the data will suffice to stipulate the nature of the effective channels and hence provide us with an ability to unfold some selective short-range dynamical aspects of great interest, such as specific polarization effects related to quark dynamics.

For the basis states $|\alpha\rangle$ in the $|\bar{p}p\rangle$ and $|\bar{n}n\rangle$ space, the potentials we adopt are essentially those developed by the Nijmegen group, who use one-boson-exchange models plus G parity to reverse the nucleon into an antinucleon line (see the Appendix for a brief description of their OBEP potential). The meson exchange part of the $\bar{N}N$ potentials in the $\bar{N}N$ sector have the following characteristics. (i) The $\bar{p}p$ and $\bar{n}n$ diagonal potentials arise from

and 4, along with the associated exchanged particles. These diagrams include the exchange of rather heavy particles, and hence, involve quite short ranges; for example, the Λ exchange corresponds to a range of ≤ 0.18 fm. That range is within the realm of quark and annihilation effects. Despite a serious concern about believing these diagrams at such short distances, they do provide some useful guidance. (It should be noted that we are using the one-hadron-exchange description for both the diagonal and transition interactions. These involve very different ranges and one could argue that at ranges where we doubt the elastic channel exchange mechanisms are where the transition potentials also breakdown. That is a valid concern, but we hope that it will prove possible to extract a fundamental short-distance transition potential, even in a zone where the diagonal potentials are uncertain, by systematically combining this CC approach with the new LEAR data.) The hadron exchange diagrams of Fig. 4 do describe the correct quantum number flow and associated selection rules; give the correct operator structure, satisfying the correct symmetries, in the baryon space; and are of the correct general range. See later for a discussion of the relationship between the range of the transition potentials and the region where annihilation occurs.

The hadron exchange diagrams lead to transition potentials which are subject to a smooth cutoff of the form given in Eq. (1), with a very small cutoff of $r'_c \approx 0.055$ fm, which was varied in fitting data. In addition to that short distance cutoff, the meson production interactions include a form factor, $F(q_M) = \Lambda^2 / (\Lambda^2 + q_M^2)$, at each meson-baryon-antibaryon vertex; here, q_M denotes the final meson's three momentum. The common value of $\Lambda = 1.0$ GeV/c was used for both pion and kaon production. For values in that range, the cross sections were not very sensitive to Λ .

In addition to the many diagrams above, we still need to look at Δ , N^* , and Y^* isobar exchange effects, at the formation of intermediate-state resonances, such as in $\bar{p}p \rightarrow \rho^*$, $\xi \rightarrow \bar{K}K$, and at the role of K^* and K^{**} mesons.

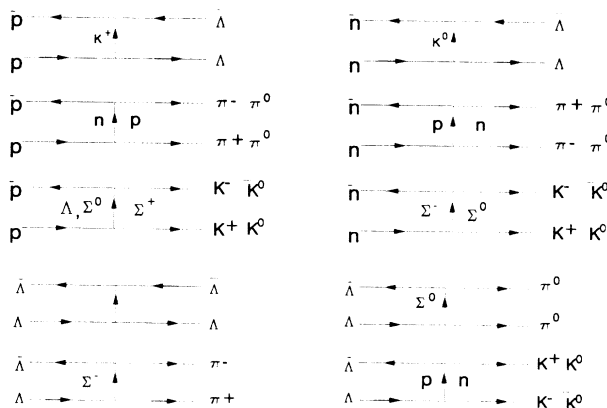


FIG. 4. Two-body channels in $\bar{p}p$ reactions—one-hadron-exchange processes. In addition to the few channels illustrated here, many other channels can be reached by $\bar{p}p$.

Such effects have been studied in the literature,^{19–21} but have not yet been fully embedded in a coupled-channels formulation. The quark diagrams, which parallel the hadron exchange diagrams, are illustrated in Fig. 5. Ideally, it is desirable to extract form factors and modified propagators from the quark model, which is clearly a very ambitious hope.

So far, ten parameters have been introduced, four strength parameters for the $\bar{p}p$ (and $\bar{n}n$) diagonal phenomenological terms and four for the $\bar{p}p \rightarrow \bar{n}n$ coupling terms; the ninth parameter is the range m_e^{-1} , which is assumed to be the same for all $\bar{p}p$ and $\bar{n}n$ terms. The tenth parameter is r_c , which cuts off the OBEP potential.

Additional parameters are needed for the $\bar{p}p$ annihilation. The Nijmegen approach is adopted to describe annihilation; i.e., instead of using optical potentials to absorb flux from the $\bar{p}p$ channel, effective particle channels are coupled to the $\bar{p}p$ and $\bar{n}n$ channels to simulate the effects of other two-body and multiparticle annihilations. The effective channels EB_i , couple to $\bar{p}p$ and $\bar{n}n$ channels in all partial waves. Couplings between these effective channels and $\bar{N}N$ channels are assumed to be of simple Woods-Saxon form,

$$V = V_{EB} [1 + \exp(m_a r)]^{-1} . \tag{5}$$

The same short-range cutoff form, was applied to all transition potentials between the antibaryon-baryon channels and the effective channels EB_i , i.e., Eq. (1) was used with the cutoff r'_c , where, for example, $r'_c \approx 0.055$ fm, for $p_{lab} = 780$ MeV/c. With r'_c the parameter count is now eleven. The EB_i channels involve an additional nine parameters, which brings the total number of free parameters used to fit the CC data to 20. The nine parameters in the EB_i case consist of four masses M_i of the effective intermediate-state particles, four strength parameters, plus one range. The 20 parameters are presented later in

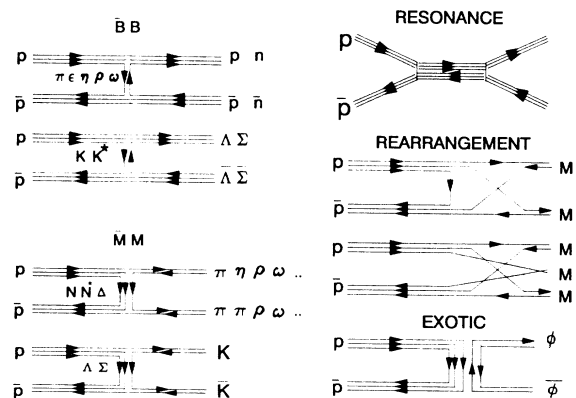


FIG. 5. Two-body channels in $\bar{p}p$ reactions—quark flow diagrams. The annihilation and production of $\bar{q}q$ pairs, resonant, quark rearrangement, and exotic intermediate and purely gluonic intermediate states are all illustrated here. Note the parallel hadronic exchange diagrams of Fig. 4. The notation adopted is $(\bar{M})M$ for (anti)mesons, $(\bar{B})B$ for (anti)baryons and $(\bar{Y})Y$ for (anti)hyperons.

Tables I and II for various case studies.

Since these effective channels describe the overall effect of many $\bar{p}p$ annihilation channels, including the dominant five-pion production process, it is not presently possible to derive the physical properties of these effective channels from simple physical arguments. The purpose of these effective channels is to absorb flux from $\bar{p}p$ states, so that the $\bar{p}p$ elastic and charge exchange reactions are properly described. With effective channels coupled in, it is also possible, but no longer necessary, to introduce complex (diagonal) potentials into the coupled system. As will be seen later, the use of effective channels, without additional complex diagonal potentials, suffices to produce rather good fits to experimental $\bar{p}p$ elastic and charge exchange differential cross sections.

At first, we did not include any explicit energy dependence in the potential parameters discussed earlier. The 20 free parameters were adjusted to fit the $\bar{p}p$ elastic and charge exchange differential cross sections at 780 MeV/c. The calculated (CAL) set CAL-I has the phenomenological tensor potential set to zero; for set CAL-II that tensor term was turned on but remained weak. Then the energy dependence of the model is explored using the parameter set CAL-II, from the 780 MeV/c fit, at other energies. Qualitatively correct behavior over a broad energy region was noted, but precision required changes in the phenomenological parameters at each energy (see the CAL-III and CAL-IV sets).

C. Selection rules

The full coupled-channels space is greatly reduced by invoking symmetries associated with parity, isospin, charge conjugation, G parity, and time reversal invariance.²² The main point is that only certain channels can be coupled. For example, the $\bar{\Lambda}\Lambda$ channel is reached by only the $I=0$ component of $\bar{p}p$. The identical meson states such as $\bar{\pi}\pi$ and $\bar{K}K$ can be reached only via the $[{}^3(L-1)_J + {}^3(L+1)_J]$ triplet-coupled $\bar{p}p$ states. The $K_S K_S$ and $K_L K_L$ states have $J=\text{even}$ and the $K_S K_L$ states have $J=\text{odd}$, assuming CP invariance. Such rules, including generalizations to ρ , ω , and η mesons, permit a considerable truncation of the coupled-channels space. Nevertheless, so many channels can couple that it paid to use a supercomputer. By invoking effective channels that couple to all states, we include the broad features of the essential annihilation effects.

D. Transition interactions—OHE

The solution of the coupled-channels equations requires that we specify the transition potentials $V_{\alpha\beta}$. They correspond to the one-hadron-exchange (OHE) processes of Fig. 4. Let us consider just one example: the one-baryon-exchange potentials (OBEP). The quark flow diagrams shown in Fig. 5, parallel the above OHE description and might eventually be used to derive transition potentials. Presently, quark model calculations²³ have not yet yielded readily usable transition potentials for two-meson channels. Therefore, at this stage we use the OHE approach and expect, based on quantum number flow and

reasonable ranges and operator content, that our interactions and those based on quark dynamics are similar in structure.

For pion production, see the hadron exchange diagrams in Fig. 4, where the charged pion case is illustrated. For neutral pions a crossed diagram must also be included. Similar diagrams hold for the production of kaons, η 's, etc. The explicit expression for the charged pion case, after expanding in p/M and Fourier transforming, leads to coordinate space transition potential operators

$$\begin{aligned} V_{BM} &= \frac{g^2}{4\pi} \frac{i}{2E_M E_B} \sigma \cdot [(\mu - M_B) \nabla Y(r) - E_B Y(r) \nabla], \\ V_{MB} &= \frac{g^2}{4\pi} \frac{i}{2E_M E_B} \sigma \cdot [\mu - M_B) Y(r) \nabla - E_B \nabla Y(r)]. \end{aligned} \quad (6)$$

Details of the derivation are given in Liu's thesis.¹⁶ These transition potentials are subject to the smooth cutoff $C(r)$ of Eq. (1), with the parameter r'_c , as discussed earlier. The procedure, based on the modification of the hadron propagator, is to replace the Yukawas by

$$Y(r) \rightarrow Y_c(r) \equiv Y(r) \times C(r).$$

That replacement, which involves derivatives of $C(r)$, is done carefully to assure the unitarity and symmetry of the S matrix, as required by flux conservation and time reversal considerations. In this case, it is important to use smooth cutoffs. The coupling constants in Eq. (6) are fixed at $g_{\pi NN}^2/4\pi = (3.66)^2$, $g_{N\Lambda K}^2/4\pi = 12.904$, and $g_{N\Sigma K}^2/4\pi = 1.2056$. (The couplings are taken from the rules

$$\begin{aligned} g_{N\Lambda K}^2/4\pi &= (g_{\pi NN}^2/4\pi)[3 - 2\alpha]^2/3, \\ g_{N\Sigma K}^2/4\pi &= (g_{\pi NN}^2/4\pi)[2\alpha - 1]^2, \end{aligned}$$

with $\alpha=0.65$.) The baryon and meson energies given earlier are fixed on-shell by the incident \bar{p} momentum. The meson-nucleon-antinucleon vertex form factors, $F(q_M)$, are included as discussed earlier. Studies of form factor effects using a momentum space CC method are under study.

The preceding spin operator involves the $\bar{N}N$ initial-state spin projections (\bar{m}_s, m_s) , in the matrix $\langle \bar{m}_s | \sigma | m_s \rangle$. Here V_{MB} acts on the $\bar{B}B$ wave function in the meson channel equation, and V_{BM} acts on the $\bar{M}M$ wave function in the baryon channel equation. (For the pion production case $B \equiv p$ and $M \equiv \pi$.)

The ∇ operator appears here as a consequence of parity, since the initial $\bar{N}N$ state has a net intrinsic parity of -1 , whereas the final two-pion state has a net intrinsic parity of $+1$. Stated another way, the transition from $\bar{N}N$ to $\pi\pi$ proceeds, for example, via

$$\bar{p}p [{}^3S_1 + {}^3D_1] \rightarrow \bar{\pi}\pi [P_{J_\pi=L_\pi=1}],$$

which requires the disappearance of spin and a spatial parity change. Thus, parity conservation requires that the two-pion production operator be odd in parity, i.e., of $\sigma \cdot \nabla$ form. This transition potential form, which arose from examination of the hadron exchange diagrams, is probably of the general form needed for all spinless

meson production transition operators. It does stipulate the potential in all partial waves, as opposed to using "local" transition potentials in each partial wave. *It is not clear that these essential gradients have been included in earlier meson and $\bar{\Lambda}\Lambda$ CC production studies in the literature.* (In Moussallam's^{24,25} fine work, such effects have been implicitly included, since he evaluates the diagrams in momentum space; however, he does not include multistep processes obtained by solving CC equations.)

To the extent that the effective channels simulate spinless meson production, the Eq. (6) form should be used for the effective-channel couplings instead of Eq. (5). However at this stage, we have not used this form for the effective channel transitions, partly for convenience and partly because it is not clear how much they simulate just the two-spinless-meson production, versus other two-meson channels, such as ρ, ω production. The general form of the transition operators for ρ, ω production is under study; indeed, we are going beyond the static limit presented here by formulating a momentum-space, CC approach built on the PIPIT code.²⁶

Having presented the potentials and their associated parameters and cutoffs, we now turn to the cross sections determined by numerical solution of the coupled-channels Schrödinger equation

$$(T_\alpha - E_\alpha + V_\alpha + V_\alpha^{\text{Coul}})\Psi_\alpha = -\sum_\beta V_{\alpha,\beta}\Psi_\beta. \quad (7)$$

Here T_α and E_α denote the kinetic energy and the kinetic-energy eigenvalue in the channel α ; V_α and V_α^{Coul} are the strong and Coulomb (diagonal) interactions in the channel α .

III. COUPLED-CHANNELS EFFECTS: THE TRUNCATED CC STUDY

As an illustration of the role of coupled-channels effects, we first discuss some results from Liu's thesis.¹⁶ The Nijmegen D potential was used with a G -parity switch, plus the phenomenological potential of Eq. (2). A fit to the Kayagama *et al.* data¹³ was achieved by adjusting V_{phen} and the cutoffs (see Ref. 16 for parameters, and other details).

To demonstrate the role of multistep processes, the coupled-channels code was used in the following manner: (i) a fit to the elastic and charge exchange data was made without coupling to meson production channels, but including V_{phen} and the effective channels EB; (ii) the $\pi^+\pi^-$ transition potential was turned on and a qualitative fit to the pion production data was made by adjusting the cutoff, r'_c , in that transition potential; (iii) the back effect of including the pion production on the elastic and the charge exchange data was examined; (iv) the preceding procedure was repeated with just the K^-K^+ channel on, then with both the K^-K^+ and $\pi^+\pi^-$ turned on; (v) the back effect of including these charged meson production channels on the elastic, charge exchange, and charged meson production cross-sections was examined.

The results of that study are given in Liu's thesis¹⁶ and also in Refs. 22, 27, and 28. The main features shown in these calculations are that (i) the elastic cross section is

not affected very much by the meson production channels, except at large angles; (ii) the charge exchange cross section is significantly more sensitive to meson channels, probably because of its dependence on the additive π and ρ meson exchange effect; (iii) the charged pion and kaon channels have a very large mutual coupling effect; (iv) the final-state $\pi\pi$ interaction needs to be included, but is not of great import, largely because of the sizable exit speed of the produced pions. (The results presented here omit the final-state $\pi\pi$ and $\bar{K}K$ interactions; they were studied to some extent in Ref. 16.) As a consequence of the preceding, it is important to include both pion and kaon channels simultaneously. We need to refit all the data, elastic, charge exchange, and both charged and neutral, strange and nonstrange, meson production simultaneously before one can reliably extract information from these reactions. Part of that full study, largely motivated by the significant role of multistep processes, is presented next.

A study of the coupled-channels effects in the $\bar{\Lambda}\Lambda$ region has also been made and the results will be presented elsewhere. In that region, one needs to include the coupling between the pions, kaons, and the Λ particles. Great sensitivity to the unknown $\bar{\Lambda}\Lambda$ potential is noted.

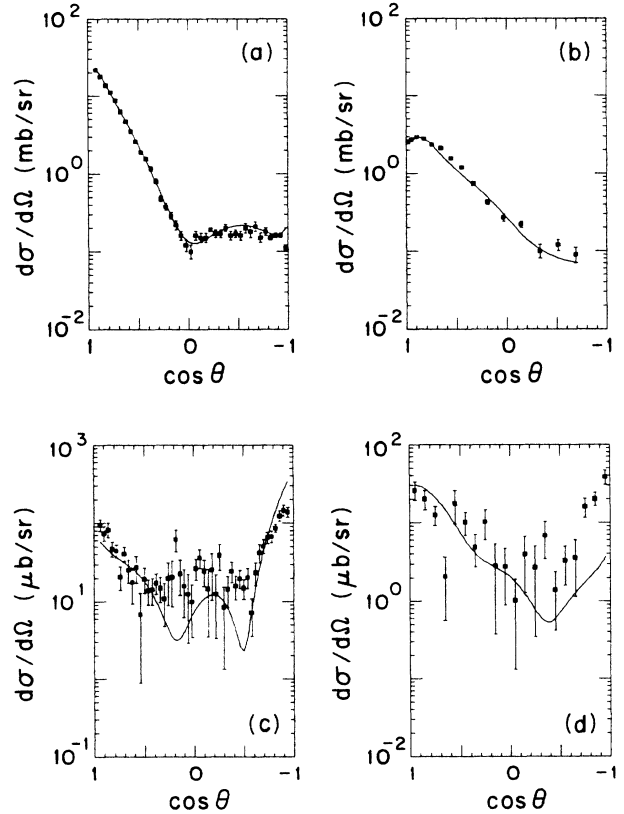


FIG. 6. Differential $\bar{p}p$ cross sections at $p_{\text{lab}} = 780$ MeV/c (lab kinetic energy: 281 MeV). (a) Elastic and (b) charge exchange data. The data are that of Eisenhandler *et al.* (Ref. 32), Kageyama *et al.* (Ref. 13), plus some from Jayet *et al.* (Ref. 33); (c) the Eisenhandler *et al.* (Ref. 32) $\pi^-\pi^+$ data; and (d) the K^-K^+ data of Eisenhandler *et al.* (Ref. 32); solid curves are the CAL-I coupled-channels results.

IV. THE LARGER CC SPACE

A. Differential cross sections

The results of the larger channel space fit to the $\bar{p}p$ elastic, charge exchange, and charged pion and kaon differential cross sections, together with the recent Kunne^{14,15} and Tanimori *et al.*²⁹ data, are presented in Figs. 6–11. The best fit parameters for the phenomenological short-range part of the $\bar{N}N$ potential and for the effective EB channels are given in Tables I and II.

The results presented in Figs. 8–11 show that the $\bar{p}p$ elastic and charge exchange differential cross sections for \bar{p}_{lab} momenta 780, 690, and 590 MeV/c can be described using meson exchange potentials as the long-range interactions, plus a phenomenological short-range potential as the short-range interactions. Also annihilation to channels other than $\bar{p}p$ and $\bar{n}n$ can be simulated by four effective channels with a simple Woods-Saxon coupling between each effective EB_{*i*} channel and the $\bar{p}p$ and $\bar{n}n$ channels. Our calculation of the $\bar{p}p$ elastic and charge exchange differential cross sections shows that the four

effective channels, EB_{*i*}, are able to generate the major effect of a multitude of $\bar{p}p$ annihilation channels back on the $\bar{p}p$ and $\bar{n}n$ channels. We also found in this model that at short distances, the $\bar{N}N$ system has very strong central and spin-orbit interactions, the strength of those phenomenological potentials ranging from about 1.5 to 5 GeV in magnitude; in contrast, the spin-spin terms are ≈ 0.3 –0.8 GeV and the tensor terms are relatively weak (see Tables I and II).

The differential cross-section results are shown in Fig. 8, for the “full fit” case; i.e., for the simultaneous fitting of the $\bar{p}p$, $\bar{n}n$, K^-K^+ , and $\pi^-\pi^+$ data in a CC approach. The elastic and charge exchange fits are quite good. The so-called “bump-dip” structure of the charge exchange data is achieved *without* a strong, phenomenological long-range tensor force. That fit is obtained largely by having noncentral effects arising from CC effects; that is, one obtains a $(\sigma_1 \cdot \nabla)(\sigma_2 \cdot \nabla)$ effect from the multistep process $\bar{p}p \rightarrow \bar{\pi}\pi \rightarrow \bar{n}n$, where the $\sigma \cdot \nabla$'s arise from the transition potentials of Eq. (6). Thus one has noncentral transitions of the type $^3S_1 \rightarrow P_1 \rightarrow ^3D_1$. This source for noncentral effects is an important difference with preceding

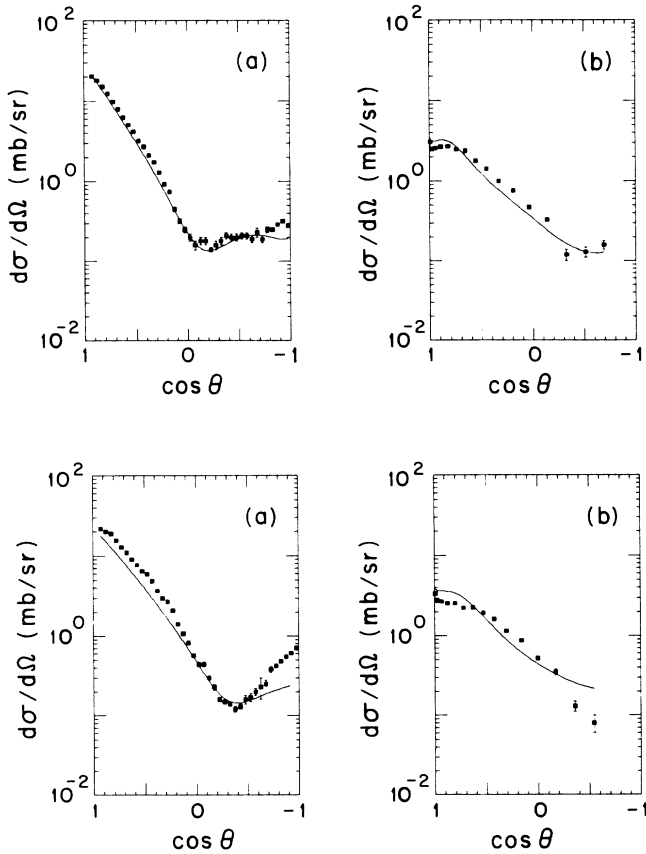


FIG. 7. Differential $\bar{p}p$ elastic (a) and charge exchange (b) cross sections at $p_{\text{lab}}=590$ MeV/c (top) and 690 MeV/c (bottom). The data used are specified in the caption to Fig. 6. Solid curves are the CAL-I coupled channels results, where CAL-I parameters are fitted to the 780 MeV/c data.

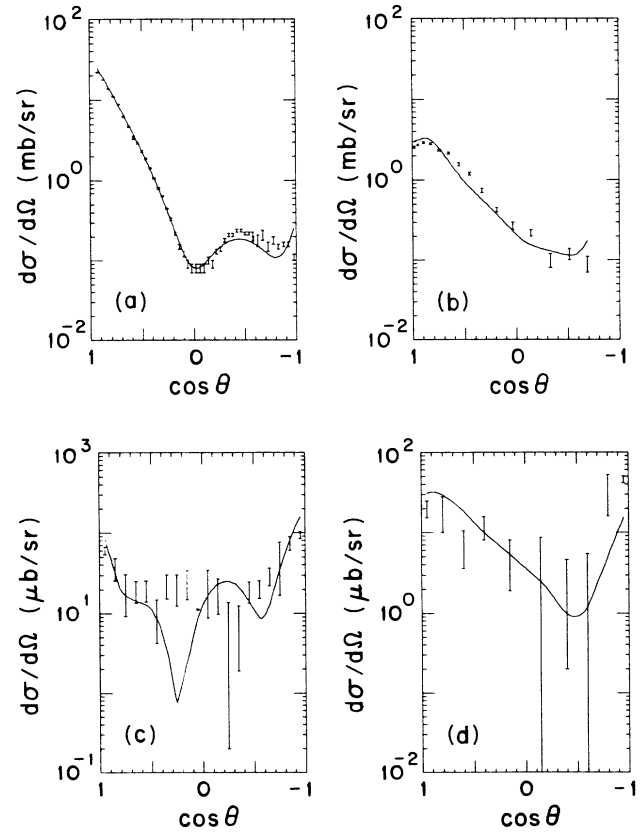


FIG. 8. Differential $\bar{p}p$ cross sections at $p_{\text{lab}}=780$ MeV/c (lab kinetic energy: 281 MeV). (a) Elastic and (b) charge exchange results. The data are now that of Kunne *et al.* (Refs. 14 and 15) for $|t| \leq 0.58$ and Eisenhandler *et al.* (Ref. 34) for $|t| > 0.58$; the (c) $\pi^-\pi^+$ and (d) K^-K^+ results with the data of Tanimori *et al.* (Ref. 29); the solid curves are the CC CAL-II results.

models.

The fit to the charged meson data is not as good. We use the recent Tanimori *et al.*²⁹ data. The back angle build up for K^-K^+ is, however, achieved (indeed, overachieved); whereas the back-angle buildup for charged pions is not adequate. These problems with back angles remain a problem for this model. Perhaps, final-state pion and kaon interactions, some resonance effects, and direct coupling of the mesons to effective channels EM_i might be needed.

The polarization at 780 MeV/c is presented in Fig. 11 for elastic and charge exchange. Comparison with the Kunne data is fair, but as is not uncommon when one tries to match both differential and total cross sections, the spin dependence is not pinned down enough to give a precision result. The availability of this polarization data provides a crucial test of $\bar{p}p$ models; we are not satisfied with the present result illustrated here and with similar

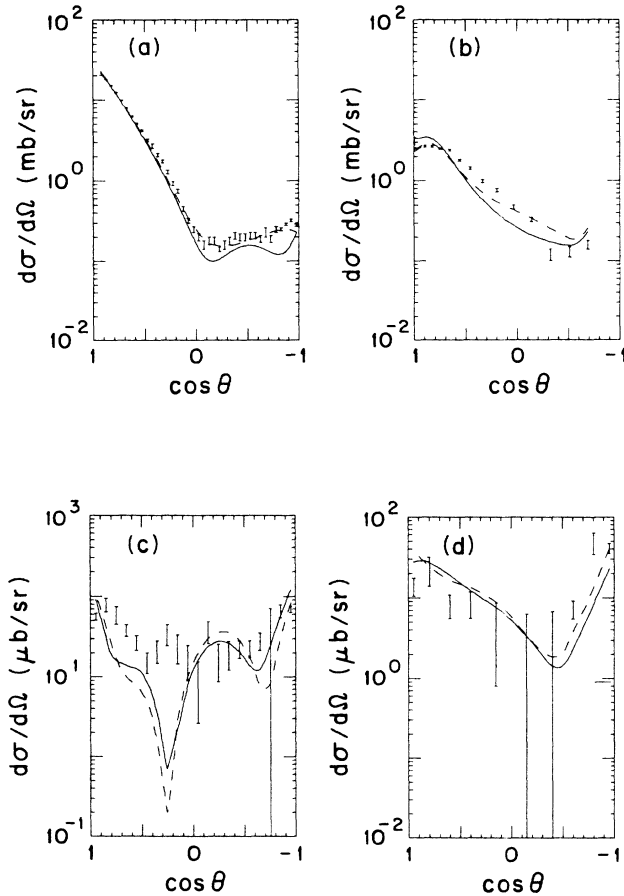


FIG. 9. Differential $\bar{p}p$ cross sections at $p_{\text{lab}} = 690$ MeV/c. (a) Elastic and (b) charge exchange data. The data are now that of Kunne *et al.* (Refs. 14 and 15) for $|t| \leq 0.58$ and Eisenhandler *et al.* (Ref. 34) for $|t| > 0.58$; (c) the $\pi^- \pi^+$ data of Tanimori *et al.* (Ref. 29); and (d) the $K^- K^+$ data of Tanimori *et al.* (Ref. 29). The solid curves are the CC results for the CAL-II parameters determined by the 780 MeV/c fit. The dashed curves are for the CAL-III set which improves the elastic and charge exchange fits.

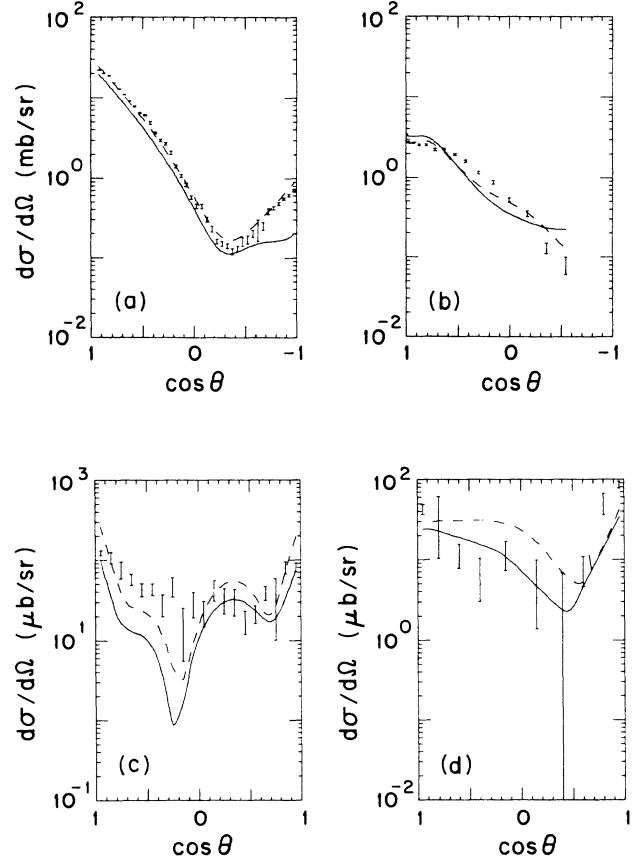


FIG. 10. Differential $\bar{p}p$ cross sections at $p_{\text{lab}} = 590$ MeV/c. (a) Elastic and (b) charge exchange data. The data are now that of Kunne *et al.* (Refs. 14 and 15) for $|t| \leq 0.58$ and Eisenhandler *et al.* (Ref. 34) for $|t| > 0.58$; (c) the $\pi^- \pi^+$ data of Tanimori *et al.* (Ref. 29), and (d) the $K^- K^+$ data of Tanimori *et al.* (Ref. 29). The solid curves are the CC results for the CAL-II parameters determined by the 780 MeV/c fit. The dashed curves are for the CAL-IV set which improves the elastic and charge exchange fits.

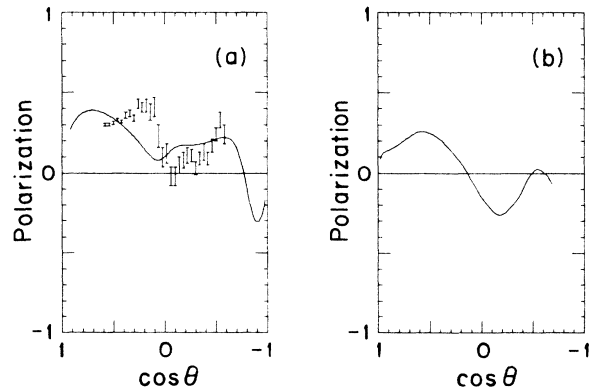


FIG. 11. Polarization of final state \bar{p} 's in elastic scattering at 780 MeV/c. The data are the analyzing power measured by Kunne *et al.* (Refs. 14 and 15). The solid curve shows the full CC result for the CAL-II parameters. The plot on the right gives the \bar{n} polarization.

TABLE I. Parameters for the short-range part of the $\bar{N}N$ potential: r_c is the cutoff of the meson exchange potentials in the $\bar{N}N$ sector; m_e is the range parameter of the Woods-Saxon used in the phenomenological short-range $\bar{N}N$ potential; $V^{(D)}$ are the strengths of the $\bar{p}p$ and $\bar{n}n$ diagonal terms; $V^{(C)}$ are the strengths of the $\bar{p}p \rightarrow \bar{n}n$ coupling terms.

P_{lab} (MeV/c)	780 MeV/c	780 MeV/c	690 MeV/c	590 MeV/c
	CAL-I	CAL-II	CAL-III	CAL-IV
r_c (fm)	1.059	0.962	1.222	1.0503
m_e (MeV)	597.88	599.87	601.92	605.57
$V_{\text{phen},C}^{(D)}$ (MeV)	-5246.7	-5259.4	-4819.1	-5019.1
$V_{\text{phen},SS}^{(D)}$ (MeV)	-378.73	-462.16	-579.72	-414.06
$V_{\text{phen},LS}^{(D)}$ (MeV)	5572.4	5593.5	5718.0	5857.2
$V_{\text{phen},T}^{(D)}$ (MeV)	0.00	92.49	259.05	346.22
$V_{\text{phen},C}^{(C)}$ (MeV)	-2917.0	-2696.9	-2644.5	-2538.7
$V_{\text{phen},SS}^{(C)}$ (MeV)	-861.42	-831.96	-812.39	-788.52
$V_{\text{phen},LS}^{(C)}$ (MeV)	-1526.3	-1331.2	-1878.1	-1241.7
$V_{\text{phen},T}^{(C)}$ (MeV)	0.00	15.34	-8.75	211.23

results at other energies²⁸ and plan to improve the spin dynamics of the model in the future.

At the two lower energies, we again use the Kunne *et al.*^{14,15} elastic and the Tanimori *et al.*²⁹ charged meson data; the results are presented in Figs. 9 and 10 and Tables I and II. Using the same parameters determined by the CC “full fit” at 780 MeV/c (CAL-II) yields reasonable, but not precision, fits at 690 MeV/c and at 590 MeV/c. Thus, the energy dependence of the model itself is not perfect and one needs to adjust the parameters at these other energies. Parameters sets CAL-III and CAL-IV, which improve the elastic and charge exchange fit, are presented for each of the three momenta considered here in Tables I and II. Significant noncentral $(\sigma_1 \cdot \nabla)(\sigma_2 \cdot \nabla)$ CC effects due to the $\bar{p}p \rightarrow \bar{\pi}\pi \rightarrow \bar{n}n$ process enter at all of these momenta.

B. Partial and total cross sections

To gain insight into the CC dynamics, we present the partial cross sections σ_J in Fig. 12 at 780 MeV/c. Note that the elastic partial cross section peaks at $J=1$, indicating a ${}^3S_1 + {}^3D_1$, 3P_1 , 1P_1 dominance. The charge exchange partial cross sections also peak at $J=1$, but have a slower falloff with J than found for the elastic σ_J . This slower falloff is partly due to the p - n mass difference, but mainly due to range effects and the ρ meson.

The pion partial cross section has little 3P_0 strength, peaks at the ${}^3S_1 + {}^3D_1$ state, and again at the ${}^3D_3 + {}^3G_3$ state, then falls rapidly. Here we see the role of the ${}^3(L \pm 1)_J \rightarrow L_J$ selection rule for pion pair production.

Only a few partial waves contribute to the K^-K^+ channel and those terms are mainly smaller than the pion

TABLE II. Effective-particle EB_i channel parameters. M_i ($i=1,2,3,4$) are the masses of the effective particles, m_a is the range parameter of the Woods-Saxon in the coupling potentials between the effective EB_i channels and $\bar{p}p$ or $\bar{n}n$; r'_c is the range of the smooth cutoff function for all transition potentials, and V_{ip} are the coupling strengths between the effective channel i and $\bar{p}p$. The V_{in} coupling strengths between the effective channel i and $\bar{n}n$ are the same as for V_{ip} , except for a sign change for the $I=1$ ($i=2$ and 4) potential parameters. Effective channels 1 and 3 have zero isospin, 2 and 4 are of isospin one.

P_{lab} (MeV/c)	780 MeV/c	780 MeV/c	690 MeV/c	590 MeV/c
	CAL-I	CAL-II	CAL-III	CAL-IV
m_a (MeV)	423.31	415.91	417.14	459.00
r'_c (fm)	0.0551	0.051	0.050	0.051
M_1 (MeV)	844.03	842.48	835.17	859.86
M_2 (MeV)	850.35	847.52	854.99	865.18
M_3 (MeV)	207.83	178.09	224.60	181.87
M_4 (MeV)	168.34	157.63	142.048	160.98
V_{1p} (MeV)	1506.05	1520.44	1624.54	1763.39
V_{2p} (MeV)	-1181.00	-1135.65	-1021.62	-1342.89
V_{3p} (MeV)	2858.25	2560.68	1870.13	2540.41
V_{4p} (MeV)	-932.71	-2925.53	-2718.75	-1562.62

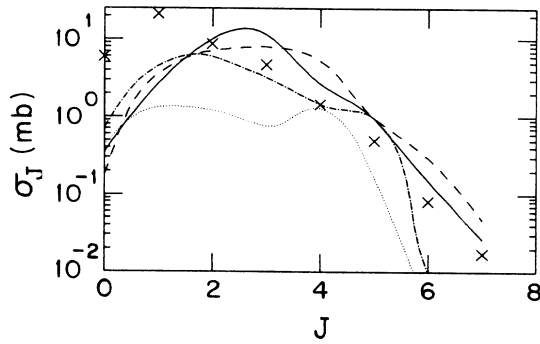
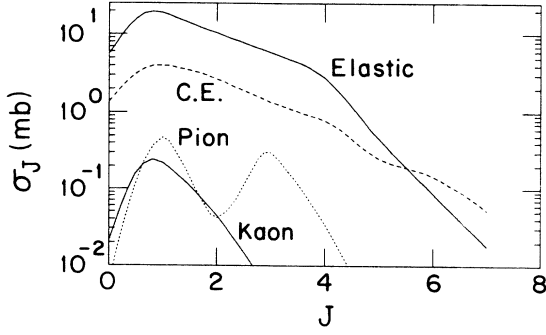


FIG. 12. Partial differential $\bar{p}p$ cross sections in millibarns at $p_{\text{lab}} = 780 \text{ MeV}/c$ (lab kinetic energy: 281 MeV). Top: partial cross sections vs J for elastic, charge exchange, and charged pion, charged kaon channels: Bottom: partial cross sections for the elastic (crosses), the effective channel EB1 (long-dash), channel EB2 (solid), channel EB3 (dot-dash), and channel EB4 (dotted). See Table II for the masses, strengths, and isospins of these effective channels.

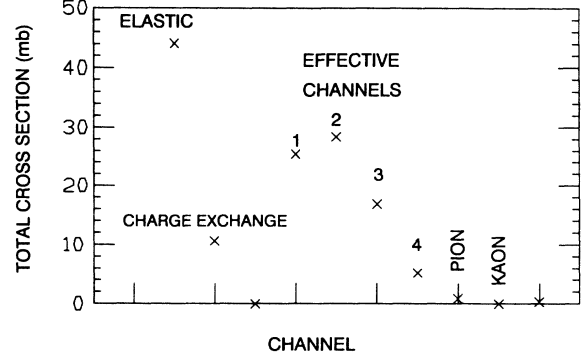


FIG. 13. Total $\bar{p}p$ cross sections at $p_{\text{lab}} = 780 \text{ MeV}/c$ (lab kinetic energy: 281 MeV) for each channel.

partial cross sections (see Fig. 12). The fact that fewer pion and kaon partial waves contribute to their total cross section than for elastic and charge exchange channels is a natural consequence of the exothermic nature of the reaction; for example, one has k^{J+1} rather than k^{2J+1} threshold behavior for exothermic reactions.

Further insight into the structure of this CC fit is also gleaned from Fig. 12, where the partial cross sections for the effective baryon channels $EB_1 \cdots EB_4$ are displayed. The crosses mark the partial cross sections for elastic scattering as a reference point. For $J=0$ (1S_0 and 3P_0 states) the individual channels are about $\frac{1}{10}$ the $\sigma_{J=0}$ (elastic), added together they are $\sim \frac{1}{5}\sigma_{J=0}$ (elastic). In contrast, at high J 's the partial EB_i cross sections are comparable or greater than σ_J (elastic), except for the ($I=1$, $M_c^2 \approx 160 \text{ MeV}$) channel which plays a smaller role. When combined as

$$\sigma^{\text{annih}} \equiv \sum_{J,i=1}^4 \sigma^J(EB_i),$$

TABLE III. The total cross sections in millibarns for $p_{\text{lab}} = 780.04 \text{ MeV}/c$ ($T_{\text{lab}} = 281.9 \text{ MeV}$). First the elastic, charge exchange, charged pions, and charged kaon channels are given, then the total cross sections for each of the four effective baryon channels are listed, along with their sum, which is the total absorption cross section. Then the total reaction cross section (i.e., the sum of the charge exchange, the charged pion, the charged kaon, and the total absorption) is given followed by the total cross section (i.e., the sum of the reaction and elastic). Other channels are assumed to be negligible. Comparison is made between the calculated (CAL) and the experimental (EXP) values. The parameter sets CAL-I and CAL-II of Table I are used here. The experimental values, where the value of p_{lab} is given in square brackets, were gleaned from Refs. 31 and 29.

Channel		σ^{tot} (mb) CAL-I	σ^{tot} (mb) CAL-II	σ^{tot} (mb) EXP
Elastic	σ_{el}	42.53	43.97	49.3 \pm 2
Charge exchange	σ_{ce}	9.44	10.62	9.26 \pm 0.1[779]
$\pi^- \pi^+$	$\sigma_{c\pi}$	1.407	0.853	0.427 \pm 0.068[772]
$K^- K^+$	σ_{cK}	0.177	0.298	0.105 \pm 0.025[772]
EB_1 ($I=0$)	σ_1	22.65	25.45	
EB_2 ($I=1$)	σ_2	26.21	28.38	
EB_3 ($I=0$)	σ_3	19.47	16.83	
EB_4 ($I=1$)	σ_4	6.078	5.167	
Absorption	σ_{ab}	74.42	75.82	
Reaction	σ_{re}	85.44	87.59	
Total	σ_{tot}	127.97	131.56	\approx 128[790]

TABLE IV. The total cross sections in millibarns for $p_{\text{lab}} = 690 \text{ MeV}/c$ ($T_{\text{lab}} = 226.4 \text{ MeV}$). First the elastic, charge exchange, charged pions, and charged kaon channels are given, then the total cross sections for each of the four effective baryon channels are listed, along with their sum, which is the total absorption cross section. Then the total reaction cross section (i.e., the sum of the charge exchange, the charged pion, the charged kaon, and the total absorption) is given followed by the total cross section (i.e., the sum of the reaction and elastic). Other channels are assumed to be negligible. Comparison is made between the calculated (CAL) and the experimental (EXP) values. The parameter set CAL-II is given in Tables I and II; these are the 780 MeV/c parameters. The CAL-III set is found by fitting at 690 MeV/c.

Channel		σ^{tot} (mb) CAL-II	σ^{tot} (mb) CAL-III	σ^{tot} (mb) EXP
Elastic	σ_{el}	45.35	45.14	53.4 ± 2.1
Charge exchange	σ_{ce}	11.65	11.33	$10.39 \pm 0.12[694]$
$\pi^- \pi^+$	$\sigma_{c\pi}$	0.77	0.69	$0.373 \pm 0.018[690]$
$K^- K^+$	σ_{cK}	0.315	0.421	$0.119 \pm 0.017[690]$
EB ₁ ($I=0$)	σ_1	26.23	24.69	
EB ₂ ($I=1$)	σ_2	29.29	30.72	
EB ₃ ($I=0$)	σ_3	18.06	13.23	
EB ₄ ($I=1$)	σ_4	5.06	3.58	
Absorption	σ_{ab}	78.65	72.22	
Reaction	σ_{re}	91.38	85.08	
Total	σ_{tot}	136.72	130.22	$126.1 \pm 5.7[694]$

the effective channels dominate over σ_J (elastic) by factors of ~ 4 . This is simply the dominance of annihilation over elastic processes.

The interesting point is that the dominance of annihilation does not set in for this CC model, until $J \geq 2$. For $J=0$ ($^3P_0, ^1S_0$) and $J=1$ ($^3S_1 + ^3D_1, ^3P_1, ^1P_1$) states, the σ_J elastic seems to stand out. It will be interesting to see if this is characteristic of the $\bar{p}p$ dynamics or is just an attribute of this particular specimen fit. The breakdown of the total cross section by channel is shown in Fig. 13, where the spread of the annihilation over the four effective channels, the smallness of the meson production, and the relative importance of the elastic, charge ex-

change, and effective channels are clearly visible. (See Tables III–V.)

C. Amplitudes

An even more detailed look at the CC dynamics is provided by the partial wave amplitudes for elastic scattering and charge exchange at 780 MeV/c (similar displays at other energies and for all of the channels are also available and of interest), which are presented in Figs. 14 and 15 versus the total angular momentum J . The key to reading these Argand plots of the T matrix is in Fig. 16. Several noteworthy aspects of the CC dynamics are seen

TABLE V. The total cross sections in millibarns for $p_{\text{lab}} = 590.0 \text{ MeV}/c$ ($T_{\text{lab}} = 170.1 \text{ MeV}$). First the elastic, charge exchange, charged pions, and charged kaon channels are given, then the total cross sections for each of the four effective baryon channels are listed, along with their sum, which is the total absorption cross section. Then the total reaction cross section (i.e., the sum of the charge exchange, the charged pion, the charged kaon, and the total absorption) is given followed by the total cross section (i.e., the sum of the reaction and elastic). Other channels are assumed to be negligible. Comparison is made between the calculated (CAL) and the experimental (EXP) values. The parameter set CAL-II is given in Tables I and II; these are the 780 MeV/c parameters. The CAL-IV set is found by fitting at 590 MeV/c.

Channel		σ^{tot} (mb) CAL-II	σ^{tot} (mb) CAL-IV	σ^{tot} (mb) EXP
Elastic	σ_{el}	46.34	58.66	$57.3 \pm 1.8[599]$
Charge exchange	σ_{ce}	12.72	12.51	$11.87 \pm 0.12[596]$
$\pi^- \pi^+$	$\sigma_{c\pi}$	0.67	1.53	$0.534 \pm 0.025[590]$
$K^- K^+$	σ_{cK}	0.341	0.510	$0.225 \pm 0.022[590]$
EB ₁ ($I=0$)	σ_1	26.23	24.78	
EB ₂ ($I=1$)	σ_2	30.02	33.88	
EB ₃ ($I=0$)	σ_3	19.62	21.36	
EB ₄ ($I=1$)	σ_4	4.99	4.66	
Absorption	σ_{ab}	80.86	84.69	
Reaction	σ_{re}	94.58	99.24	
Total	σ_{tot}	140.92	157.90	$154.3 \pm 3[599]$

here. First note that the coupled states do split with, for example, the 3S_1 larger than its partner 3D_1 state, at least for their imaginary parts. However, the $S \rightarrow D$ type transitions yield small amplitudes, suggesting a cancellation between the various sources of noncentral effects. It is also of interest to compare the coupled-state amplitudes for the elastic and charge exchange cases; compare Fig. 14 to Fig. 15. For charge exchange, noncentral $J-1 \rightarrow J+1$ transitions are still small, but the diagonal $J \pm 1 \rightarrow J \pm 1$ amplitudes are quite different from the elastic case, which is no surprise since only isospin 1 (π and ρ) mesons are involved in charge exchange. It is significant that the “bump-dip” structure of charge exchange is reproduced without strong tensor forces, mainly because of CC effects such as the appearance of the operator $\sigma \cdot \nabla \sigma \cdot \nabla$ due to multistep processes.

For the uncoupled transitions, the singlet and the triplet $J=L$ states, the T matrix elements fall smoothly to zero, with the charge exchange appreciably smaller. The elastic T matrix is negative, which is not indicative of a repulsion (after all the $\bar{N}N$ potential is very attractive), but rather results from possible bound-state pole and/or CC annihilation effects. (Recall that $t \approx -T \approx -(1 - VG_0)^{-1}V$, where the inverse operator depends on bound-state and absorptive effects.) For higher J , the real part of T does become positive due to the attractive nature of the $\bar{N}N$ potential (and applying the Born approximation for high J).

We can also see that several partial waves make sizable contributions to the $\bar{p}p$ elastic scattering at 780 MeV/c,

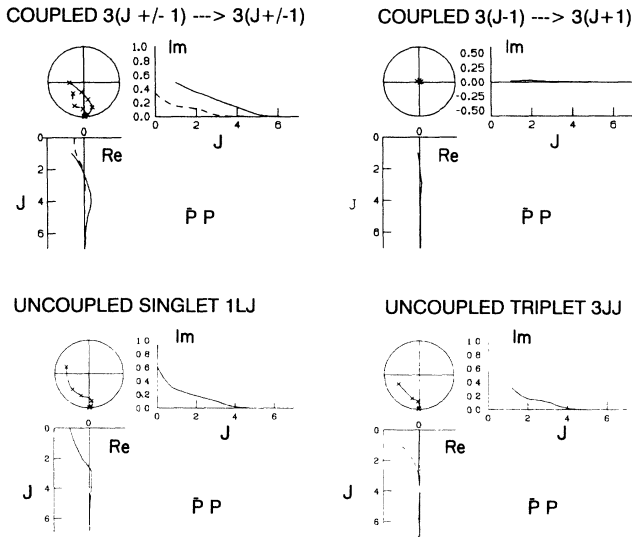


FIG. 14. Argand diagrams for elastic amplitudes at $p_{\text{lab}} = 780$ MeV/c (lab kinetic energy: 281 MeV). The real and imaginary parts of the partial wave scattering amplitudes are displayed vs J . See Fig. 16 for the key to reading these Argand diagrams. For the coupled case on top, dashed curves are for ${}^3(L+1)_J$ states and the solid are for the ${}^3(L-1)_J$ states. The label “Coupled $3(J \pm 1) \rightarrow 3(J \pm 1)$ ” denotes the $\langle {}^3(L \pm 1)_J | T_J | {}^3(L \pm 1)_J \rangle$ and the label “Coupled $3(J-1) \rightarrow 3(J+1)$ ” denotes the $\langle {}^3(L-1)_J | T_J | {}^3(L+1)_J \rangle$ amplitudes. The lower plots give the uncoupled singlet 1L_J and triplet 3J_J states.

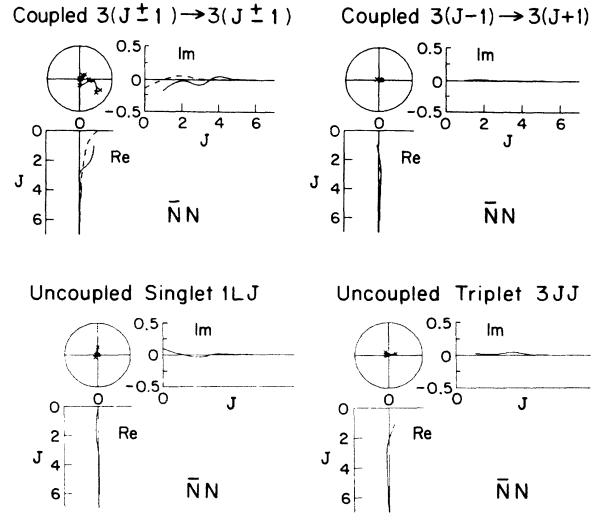


FIG. 15. Argand diagrams for charge exchange amplitudes at $p_{\text{lab}} = 780$ MeV/c (lab kinetic energy: 281 MeV). See the caption for Fig. 14.

most importantly the $L < 4$ partial waves, but major contributions to the $\bar{p}p \rightarrow \bar{n}n$ reaction come from only a few partial waves, i.e., 3P_0 and 3S_1 . Only a few partial waves dominate charge exchange since the $\bar{p}p$ system annihilates into specific channels as a result of the parity conservation; i.e., $\pi^+\pi^-$ states couple only to $L = J \pm 1$ $\bar{p}p$ states.

It would be of interest to compare the CC amplitudes presented here to those found from single-channel and absorptive disk models. From some information kindly made available to us by J. M. Richard and F. Myhrer, we conclude that those models provide amplitudes similar to the CC case.

D. Ranges and region of annihilation

The amplitudes just discussed also display the absorptive nature of the $\bar{N}N$ reaction. Clearly, the amplitudes are well within the unitarity circle drawn in Figs. 14–16.

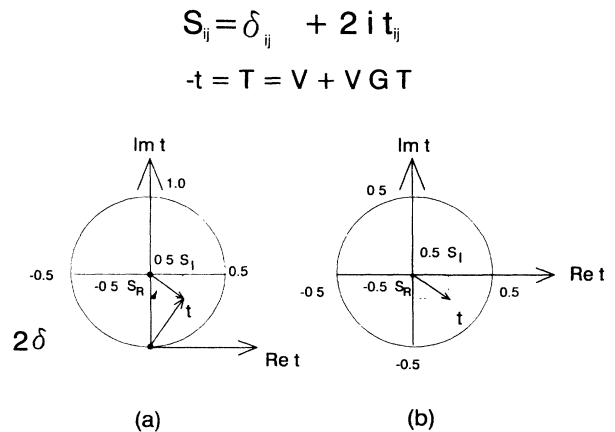


FIG. 16. Argand diagram amplitude plot. The key to reading the real and imaginary parts of the partial wave scattering amplitudes are displayed for the elastic (a) and for charge exchange (b) cases.

An interesting question is where in space does the annihilation occur. Our transition potentials are all of quite short range. See Fig. 17 for a comparison of the various ranges that enter into this problem. Does the short range of the transition potentials imply that the annihilation occurs at short distances? Let us look at the wave functions of Fig. 18, obtained from the CC study, for some guidance. Even better, from these wave functions we can construct the divergence of the radial current and use $\nabla \cdot \mathbf{j} = S(r)$ to deduce the dominant annihilation region. For positive $S(r)$, we have creation and for negative $S(r)$ we have a region of annihilation (note we use a time independent description). Thus from Fig. 18, where the source function $r^2 S(R)$ is plotted versus distance, we see that the annihilation occurs in the 0.8–1.0 fm region, but is very state dependent. There are also regions where flux is not just lost from the elastic channel, but is also fed back in from the intermediate meson (mainly pion) and the lower mass EB channels. That creative flux shows up at short distances and also in the tail region for the 1S_0 state in Fig. 18. The “creation” in the elastic channel arises in a CC approach from formation and then propagation in an intermediate state, followed by a return to the elastic channel at, say, larger distances. This is basically an effective optical potential effect of the type

$$U_{\text{opt}} \approx V \frac{1}{\epsilon} V. \quad (8)$$

The propagation range is determined by the pion’s de Broglie wavelength, about 1.2 fm, and also by the de Broglie wavelength of the lowest mass EB channel, also about 1.2 fm. Although there are creative regions due to this spatial feedback mechanism, the overall process is clearly absorptive, as was already seen from the Argand diagrams and from the attenuation of the wave functions in Fig. 18.

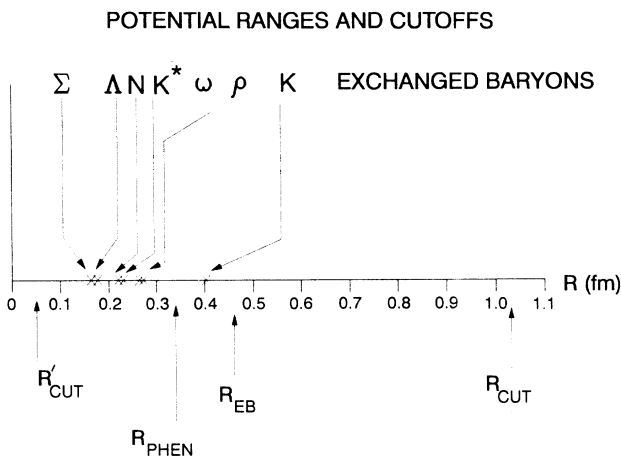


FIG. 17. The ranges involved in the coupled-channels dynamics. Here R_{CUT} denotes the parameter r_c used to cut off the OBEP potential; R'_{CUT} is the meson production transition potential cutoff r'_c . R_{PHEN} denotes the range $1/m_e$ of the phenomenological potential, R_{EB} is $1/m_a$, the range of the effective baryon transition potential. The ranges associated with the various hadron exchanges are also indicated.

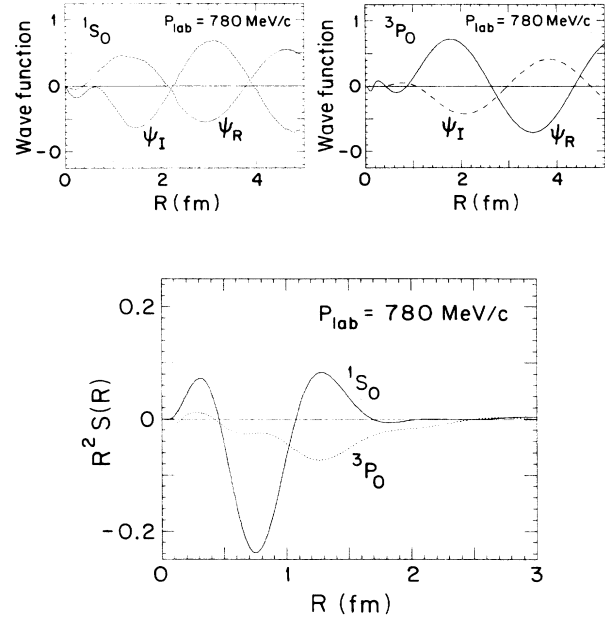


FIG. 18. (a) The radial wave functions. (b) The associated radial source function $r^2 S(r)$. Here positive values of $r^2 S(r)$ are creative, negative values absorptive regions.

We conclude that the ranges of the interactions are small, but that the region of annihilation is not so small. Indeed, the annihilation is state dependent and can have a rather long range as, for example, in the 3P_0 state of Fig. 18. Recently, Haidenbauer *et al.*³⁰ have come to related conclusions.

V. CONCLUSION

This exploratory study of a coupled-channels approach to $\bar{p}p$ reactions has led us to hope that we can deal both with the significant effects of annihilation and with the strong interaction coupled-channel dynamics. The agreement with the new data is encouraging, but as that data base develops there is a need to confront it with precision models. The effect of meson production back on the elastic and charge exchange channels needs to be included, especially in view of the newer precision made possible by LEAR. The polarization data has not been fully presented and it needs to be studied in detail, especially if one hopes to relate spin effects to underlying quark dynamics. Some indication of the nature of spin effects from CC effects has been examined here, namely, that spin effects arise not only from meson exchange, but also from the spin dependence of transition operators and from associated CC multistep effects.

Clearly, much more needs to be done. Preliminary examination of higher energies has revealed a breakdown of the present CC coordinate space model.²⁸ That has led us to improve the formulation to include nonstatic effects by applying momentum-space techniques to the $\bar{p}p$ problem.

ACKNOWLEDGMENTS

The authors are grateful to Professor R. A. Eisenstein, Professor A. M. Green, and Professor S. A. Dytman for their help and advice. One of us (G.Q.L.) would like to thank the Research Institute for Theoretical Physics, Helsinki for their hospitality. Dr. C. B. Dover and Dr. V. Girija provided several very helpful remarks for which we are thankful. We also appreciate insightful suggestions made by Professor N. Austern, Professor L. Willets, and Professor M. Alberg. This research was supported in part by the U.S. National Science Foundation and The Pittsburgh Supercomputing Center.

APPENDIX: THE NIJMEGEN POTENTIAL

We adopt the G -parity transformed Nijmegen Model- D ^{5,4} one-boson-exchange (OBE) Nucleon-Nucleon potential for the $\bar{N}N$ interaction. This potential includes exchange of π , ρ , η , η' , ω , ϕ , and ϵ mesons, where ρ and ω

are treated as broad resonances in a two-pole approximation. See Nagels *et al.*⁵ for a discussion of how they represent the broad ρ and ϵ resonances by modified meson propagators, then in r space as a mass distribution of Yukawas, and finally as a combination of two Yukawas of weights $\beta_{1,2}$ and masses $m_{1,2}$. As a result the ρ meson's OBEP is of the form $\beta_1 V_\rho(m_1) + \beta_2 V_\rho(m_2)$, where V_ρ is the vector meson exchange form that follows. A similar combination is used for the ϵ 's OBEP. Table VI summarizes the quantum numbers of the exchanged mesons. The pole parameters for ρ and ϵ are given in the bottom part of the table.^{5,4}

The coordinate space NN potentials have the following forms for isospin-zero meson exchange.

(1) Pseudoscalar meson exchange (η, η'):

$$V_{\text{ps}}^{NN} = \frac{g^2}{4\pi} \frac{1}{12MM'} [S_{12}t(r) + \mu^2(\sigma_1 \cdot \sigma_2)y(r)] \quad (\text{A1})$$

(2) Vector meson exchange (ϕ, ω):

$$\begin{aligned} V_{\text{vec}}^{NN} = & \frac{1}{4\pi} \left\{ \left[g^2 \left(1 + \frac{\mu^2}{8MM'} \right) + \frac{gf\mu^2}{2W(MM')^{1/2}} + \frac{f^2\mu^4}{16W^2MM'} \right] y(r) \right. \\ & + \frac{1}{3} \left[\frac{g^2}{4MM'} + \frac{gf}{2W(MM')^{1/2}} + \frac{f^2}{4W^2} \left(1 + \frac{\mu^2}{8MM'} \right) \right] [2\mu^2(\sigma_1 \cdot \sigma_2) - S_{12}t(r)] \\ & - \left[\frac{3g^2}{2MM'} + \frac{2gf}{W(MM')^{1/2}} + \frac{3\mu^2 f^2}{8W^2MM'} \right] s(r) \mathbf{L} \cdot \mathbf{S} \\ & \left. + \left[\frac{g^2}{16M^2M'^2} + \frac{gf}{2W(MM')^{3/2}} + \frac{f^2}{2W^2MM'} \right] \frac{t(r)}{r^2} Q_{12} \right\}. \end{aligned} \quad (\text{A2})$$

(3) Scalar meson exchange (ϵ):

$$V_{\text{scal}}^{NN} = \frac{g^2}{4\pi} \left[- \left[1 - \frac{\mu^2}{8MM'} \right] y(r) - \frac{1}{2MM'} s(r) \mathbf{L} \cdot \mathbf{S} - \frac{1}{16M^2M'^2} \frac{t(r)}{r^2} Q_{12} \right], \quad (\text{A3})$$

TABLE VI. The exchange mesons and meson pole parameters. The pion mass is the average $(2m_{\pi^+} + m_0)/3$; experimental widths are in brackets. The ϵ meson is an effective scalar meson, not the $S(975)$. All input presented here is from Refs. 5 and 4. The G -parity rule is $G = (-1)^{J+S}$.

	m (MeV)	Γ (MeV)	I	J^π	G	$g/\sqrt{4\pi}$	$f/\sqrt{4\pi}$
π	138.041	0	1	0^-	—	3.66	
ρ	770	146[154±5]	1	1^-	+	0.594 44	4.816 96
η	548.8	0[0.83±0.12 keV]	0	0^-	+	2.729 67	
η'	957.50	0[0.29±0.05]	0	0^-	+	3.887 86	
ω	783.9	0[9.9±0.3]	0	1^-	—	3.373 08	2.339 920
ϕ	1019.5	0[4.22±0.13]	0	1^-	—	-1.241 2	-0.510 04
ϵ	760	640	0	0^+	+	5.032 08	

	meson pole parameters			
	m_1 (MeV)	β_1	m_2 (MeV)	β_2
ρ	628.74	0.158 74	878.18	0.783 21
ϵ	508.52	0.199 86	1043.79	0.552 41

where

$$y(r) = \frac{e^{-\mu r}}{r},$$

$$s(r) = \left[\frac{1}{r^2} + \frac{\mu}{r} \right] \frac{e^{-\mu r}}{r},$$

and

$$t(r) = \left[\frac{3}{r^2} + \frac{3\mu}{r} + \mu^2 \right] \frac{e^{-\mu r}}{r}.$$

M, M' are the nucleon masses, μ the mass of the exchanged meson, g, f are coupling constants, W the scaling mass for f which is taken to be the proton mass.

For isospin-1 (π, ρ) meson exchange, the potential functions should be modified by multiplying by the isospin operator $\tau_1 \cdot \tau_2$. Since we work in particle basis, the operator $\tau_1 \cdot \tau_2$ needs to be projected out so that particle basis potentials can be obtained. The projection can be

done by using the relation $\tau_1 \cdot \tau_2 = P_1 - 3P_0$, where P_1 and P_0 are projection operators of total spin 1 and 0, and

$$\begin{aligned} |\bar{p}p\rangle &= -\frac{1}{\sqrt{2}}(|\bar{N}N; I=0, I_3=0\rangle - |\bar{N}N; I=1, I_3=0\rangle), \\ |\bar{n}n\rangle &= -\frac{1}{\sqrt{2}}(|\bar{N}N; I=0, I_3=0\rangle + |\bar{N}N; I=1, I_3=0\rangle). \end{aligned} \quad (\text{A4})$$

We obtain

$$\langle \bar{p}p | \tau_1 \cdot \tau_2 | \bar{p}p \rangle = \langle \bar{n}n | \tau_1 \cdot \tau_2 | \bar{n}n \rangle = -1$$

and

$$\langle \bar{p}p | \tau_1 \cdot \tau_2 | \bar{n}n \rangle = -2.$$

Therefore, the meson exchange potentials on the particle basis can be obtained from combination of the preceding basic potential forms by incorporating the G parity of both isospin-0 and -1 mesons and factors -1 (for diagonal) and -2 (for $\bar{p}p \leftrightarrow \bar{n}n$ transition potentials) for isospin-1 mesons.

*Present address: Research Institute for Theoretical Physics, University of Helsinki, Siltavuorenpenger 20C, Helsinki 17, Finland.

¹R. A. Bryan and R. J. N. Phillips, Nucl. Phys. **B5**, 201 (1968).

²C. B. Dover and J. M. Richard, Phys. Rev. C **21**, 1466 (1979).

³J. Cote *et al.*, Phys. Rev. Lett. **48**, 1319 (1982).

⁴P. H. Timmers *et al.*, Phys. Rev. D **29**, 1928 (1984).

⁵M. M. Nagels *et al.*, Phys. Rev. D **12**, 744 (1975).

⁶F. Myhrer and J. Wroldsen, Phys. Lett. B **174**, 366 (1986).

⁷A. M. Green and J. A. Niskanen, in *Progress in Particle and Nuclear Physics*, edited by A. Faessler (Pergamon, New York, 1987), Vol. 18, p. 93.

⁸F. Myhrer and R. Tegen, Phys. Lett. **162B**, 237 (1985).

⁹M. Maruyama and T. Ueda, Prog. Theor. Phys. **78**, 841 (1987).

¹⁰T. Hippchen, K. Holinde, and W. Plessas, Phys. Rev. C **39**, 761 (1989).

¹¹O. Dalkarov, K. Protasov, and I. Shapiro, P. N. Lebedev Physical Institute, U.S.S.R., Report 37, 1988.

¹²J. A. Niskanen, in *Physics at Lear with Low Energy Antiprotons*, Proceedings of the Fourth LEAR Workshop, edited by C. Amsler, G. Buckenstoss, R. Klapisch, C. Leluc, D. Simon, and L. Tauscher (Harwood Academic, New York, 1988).

¹³T. Kageyama *et al.*, Phys. Rev. D **35**, 2665 (1987).

¹⁴R. A. Kunne, PhD thesis, Universiteit van Amsterdam, 1988.

¹⁵R. A. Kunne *et al.*, Phys. Lett. B **206**, 557 (1988).

¹⁶G. Q. Liu, PhD thesis, University of Pittsburgh, 1987.

¹⁷G. Q. Liu and F. Tabakin (unpublished).

¹⁸F. Tabakin, in *Anti-Nucleon Physics*, Proceedings of the Conference on Antinucleon and Nucleon-Nucleus Interac-

tions, Telluride, Colorado, edited by G. E. Walker, C. D. Goodman, and C. Olmer (Plenum, New York, 1985), p. 471.

¹⁹R. A. Eisenstein and F. Tabakin, Phys. Rev. C **31**, 1857 (1985).

²⁰V. Girija and F. Tabakin, Phys. Rev. C **34**, 1798 (1986).

²¹M. Kohno and W. Weise, Phys. Lett. B **179**, 15 (1986).

²²F. Tabakin, in *Spring School on Medium and High Energy Nuclear Physics*, edited by W. P. Hwang (World Scientific, Singapore, 1988).

²³A. M. Green and G. Q. Liu, Nucl. Phys. **A486**, 581 (1988).

²⁴B. Moussallam, Nucl. Phys. **A407**, 413 (1983).

²⁵B. Moussallam, Nucl. Phys. **A429**, 429 (1984).

²⁶R. A. Eisenstein and F. Tabakin, Comput. Phys. Commun. **12**, 237 (1976).

²⁷F. Tabakin, *Strange particle production in antinucleon-nucleon reactions*, in *International conference on Medium and High Energy Nuclear Physics*, edited by W. P. Hwang (World Scientific, Singapore, 1988).

²⁸F. Tabakin, *Antinucleon-nucleon reactions*, in *4th Workshop on Perspectives in Nuclear Physics at Intermediate Energy—Trieste, Italy*, edited by S. Boffi *et al.* (World Scientific, Singapore, 1989).

²⁹T. Tanimori *et al.*, Phys. Rev. Lett. **55**, 1837 (1985).

³⁰J. Haidenbauer, T. Hippchen, K. Holinde, and J. Speth (unpublished).

³¹V. Flaminio *et al.*, CERN Report CERN-HERA 84-01, 1984.

³²E. Eisenhandler *et al.*, Nucl. Phys. **B96**, 109 (1975).

³³B. Jayet *et al.*, Nuovo Cimento **45A**, 371 (1978).

³⁴E. Eisenhandler *et al.*, Nucl. Phys. **B113**, 1 (1976).